

The formation of ice sails

A. C. Fowler & C. Mayer

To cite this article: A. C. Fowler & C. Mayer (2017) The formation of ice sails, *Geophysical & Astrophysical Fluid Dynamics*, 111:6, 411-428, DOI: [10.1080/03091929.2017.1370092](https://doi.org/10.1080/03091929.2017.1370092)

To link to this article: <http://dx.doi.org/10.1080/03091929.2017.1370092>



Published online: 15 Sep 2017.



Submit your article to this journal [↗](#)



Article views: 35



View related articles [↗](#)



View Crossmark data [↗](#)



The formation of ice sails

A. C. Fowler^{a,b} and C. Mayer^c

^aMACSI, University of Limerick, Limerick, Ireland; ^bOCIAM, University of Oxford, Oxford, UK; ^cBavarian Academy of Sciences and Humanities, Commission for Glaciology, Munich, Germany

ABSTRACT

Debris-covered glaciers are prone to the formation of a number of supraglacial geomorphological features, and generally speaking, their upper surfaces are far from level surfaces. Some of these features are due to radiation screening or enhancing properties of the debris cover, but theoretical explanations of the consequent surface forms are in their infancy. In this paper we consider a theoretical model for the formation of “ice sails”, which are regularly spaced bare ice features which are found on debris-covered glaciers in the Karakoram.

ARTICLE HISTORY

Received 18 January 2017
Accepted 17 August 2017

KEYWORDS

Ice sails; Karakoram; instability; supraglacial geomorphology; debris-covered glaciers

1. Introduction

Debris-covered glaciers are a widespread glacier type, especially in Central Asia and the Himalayan–Karakoram range (Benn *et al.* 2012, Bolch *et al.* 2012). Due to melt-out of englacial debris or the deposition of rock fall from mountain slopes, debris accumulates along the glacier tongues with ongoing melt (Nakawo *et al.* 1986, Rowan *et al.* 2015). These debris layers usually start as very thin layers and become thick packs of a large variety of grain sizes; they can be up to several metres thick at the glacier terminus. While very thin debris cover enhances the melt rate compared to clean ice, thick debris cover reduces melt (Östrem 1959). Due to the influence of this differential melt and the action of moving melt water on the glacier surface, the debris cover is usually not homogeneous, but shows a spatial variability (Nicholson and Benn 2013). Melt water streams and supraglacial ponds cut into the ice and generate ice cliffs which consist of bare ice, or which are covered with only a very thin layer of dust (Juen *et al.* 2014). Ice cliffs exposed to the south are usually small, because their low slope angles lead to a fast coverage with debris. In contrast, northerly exposed cliffs show steep slopes, where debris cannot accumulate, but slides off (Sakai *et al.* 2002). Ice cliff ablation became a focus of several research studies recently, due to its potential impact on the general melt rate (e.g. Reid and Brock 2014, Steiner *et al.* 2015, Brun *et al.* 2016). Ice cliffs generally experience higher melt rates than the flat debris-covered parts, and thus they enhance the large-scale surface roughness of debris-covered glacier tongues (Mayer *et al.* 2006). On steep sections of the glaciers, supraglacial debris is redistributed by mass movement, which adds to the non-regular distribution of debris and in consequence the non-uniform ice melt across the glacier tongue (Sakai *et al.* 2002).



Figure 1. Ice sails are large, quasi-tabular wedges of clean ice which protrude from the debris-covered surface of the ice. Photograph: A. Lambrecht, 2011.



Figure 2. The ice sails on Baltoro Glacier form a regular train which progresses down glacier, and extends over a distance of some 9 km. Photograph: C. Mayer, 2013.

Therefore, debris-covered glaciers usually show a rough surface topography which is very dynamic with time.

Glaciers, mainly in the Karakoram, present an additional feature on the debris-covered surface which we call “ice sails” (Mayer *et al.* 2006; figure 1): the almost continuous debris surface is interrupted by clean ice sections which resemble steep pyramidal bodies, elevated from the debris surface. These features often seem to occur in a regular sequence (figure 2), rising from the surface in the region where debris bands on the glacier merge. They increase in height on their way downstream, reaching a vertical size of up to 20 m and

horizontal dimensions of 30–40 m, before they disappear again. It seems surprising that these ice sails survive, since melt rates of clean ice should be much higher than ice melt of the surrounding debris-covered area. In addition, an extensive survey of glaciers worldwide reveals that these surface features exist mainly on the glaciers of the central Karakoram. There they usually occur at altitudes between 4000 and 4500 m. A more detailed description about morphology and regional occurrence of ice sails is given in [Evatt *et al.* \(2017\)](#).

Ice sails, also known as ice pyramids ([Fisher 1950](#), [Visser 1932](#)), are just one of a number of similar features found on debris-covered glaciers. Like the much smaller scale *penitentes* ([Lliboutry 1954](#), [Kotlyakov and Lebedeva 1974](#)), they are associated with arid conditions in which mass wastage may be by sublimation. Dirt cones ([Swithinbank 1950](#)) are similar features, but the rôle of clean ice and debris cover is reversed: dirt cones are covered with a layer of debris which prevents melting, while evidently the ice sails do the opposite: the clean ice has lower mass wastage rate.

In this paper we provide a simple mathematical model which is able to explain how differential melting of debris-covered and clean ice can lead through an instability to the formation of isolated mounds of clean ice. Up to now the origin of ice sails has not been explained, and this is a suitable way to explain their formation. Although we focus here on ice sails, the basic structure of our model may have applications in describing other such features, such as ice cliffs. The instability mechanism is based on the classical Östrem curve ([Östrem 1959](#)) which suggests that the melt rate at the surface of a glacier, considered as a function of debris thickness h , first increases with thickness before then decreasing at large h . The maximum growth rate occurs at a depth which Östrem estimated at ~ 0.5 cm, but his experimental results were based on a uniform sand cover, whereas in practice the debris cover is patchy and of irregular grain size. In addition, it is observed on Baltoro Glacier (see figure 1) that melting of clean ice is significantly lower than that of the surrounding debris-covered ice, which may have a typical thickness of several centimetres (the basal apron scarp visible in figure 1 is of height one metre, and arises precisely through excessive summer melting of the debris-covered ice). We will show that if the melt rate is an increasing function of debris cover thickness, at least for thin debris cover, then a uniform such cover is unstable, and finite width sails are then predicted by the model.

2. Mathematical model

2.1. The Östrem curve

We first describe a simple model which describes the melt rate M of debris-covered ice as a function of debris depth h . A more complex version of this model has recently been proposed by [Evatt *et al.* \(2015\)](#). As shown in figure 3, we consider a debris layer of depth h in which the solid fraction is ϕ . Below the debris layer is ice, on top of which we suppose melting causes the formation of a thin water film of (small) depth h_w . The (absolute) temperature at the surface of the layer is T , and that at the water surface is T_w . The net average incoming radiation (both short wave and scattered long wave) is denoted by Q_i ; we suppose this is absorbed at the upper surface. Similarly, the outgoing black body radiation from the upper surface is σT^4 . Additionally, there is a conductive heat flux $k(T - T_w)/h$ through the debris (here k is the relevant thermal conductivity, and we can assume a steady state as the thermal time scale is only 100 s if $h \sim 10$ cm, assuming a normal thermal diffusivity of $\sim 10^{-6}$ m² s⁻¹). There is also a sensible heat flux to the atmosphere,

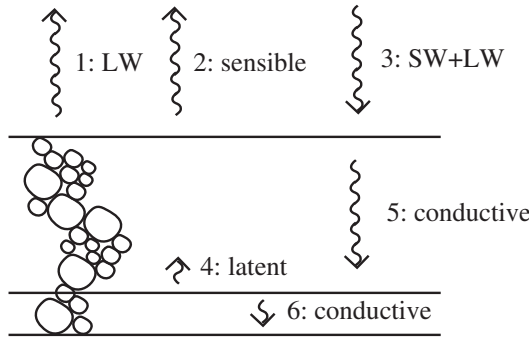


Figure 3. Energy fluxes in a debris layer. These are 1: long wave radiation out; 2: sensible heat flux to the atmosphere; 3: short wave and reflected long wave in; 4: latent heat of evaporation; 5: heat conduction through the debris; 6: heat conduction through the water film. The latent heat flux 4 occurs at the water surface, but does not contribute to the energy exchange at the debris surface as the vapour flux is continuous there.

which we take to be $h_T(T - T_a)$, where h_T is a heat transfer coefficient and T_a is atmospheric temperature, and a net heat flux Q_w through the water film. We assume for simplicity that the water film is sufficiently thin that we can take $T_w = T_M$, the melting temperature, throughout. Energy balances at the three interfaces then lead to the equations

$$\begin{aligned}
 Q_i - \sigma T^4 &= \frac{k(T - T_M)}{h} + h_T(T - T_a), \\
 \frac{k(T - T_M)}{h} - \rho_w L_v E &= Q_w, \\
 E &= \frac{\kappa_E(1 - r_h)}{h}, \\
 Q_w &= \rho_i L_m M,
 \end{aligned}
 \tag{1}$$

in which E is the evaporation rate of the water film, L_v and L_m are the latent heats of vapourisation and melting, M is the melt rate of the ice surface, r_h is the relative humidity, and κ_E is an effective moisture diffusion coefficient through the debris layer. There is evidently a singularity in the definition of the evaporation E when $h \rightarrow 0$. As we describe further below, the water film will actually vanish if E is too large, but also the singularity will be modified when $h \rightarrow 0$, since there will be a residual boundary layer in the atmosphere which prevents E becoming infinite.

On the first of these points, the water film thickness is described in this spatially independent case by

$$\rho_w \dot{h}_w = \rho_i M - \rho_w E.
 \tag{2}$$

This allows for the film to vanish if $\rho_i M < \rho_w E$, in which case sublimation would occur. If, on the other hand, $\rho_i M > \rho_w E$, the film would thicken and flow somewhat analogously to an overland flow, subject to an approximate water flux

$$\mathbf{q} = -\frac{\rho_w g h_w^3}{3\eta_w} \nabla(s + h_w),
 \tag{3}$$

Table 1. Values of the parameters used. The choices for Q_i , Q_E , h_E and h_a are discussed in the text.

Symbol	Meaning	Typical value
h	debris depth	1–10 cm
h_a	heat transfer layer thickness	10 cm
h_a^*	given by (11)	6.3 cm
h_E	moisture layer thickness	0.2–2 cm
h_T	heat transfer coefficient	$10 \text{ W m}^{-2} \text{ K}^{-1}$
k	thermal conductivity	$1 \text{ W m}^{-1} \text{ K}^{-1}$
L_m	latent heat of melting	$3.3 \times 10^5 \text{ J kg}^{-1}$
L_v	latent heat of vapourisation	$2.5 \times 10^6 \text{ J kg}^{-1}$
M_E	evaporative rate coefficient	13.3 m y^{-1}
M_E^*	annualised average of M_E	3.6 m y^{-1}
M_T	melt rate coefficient	25.7 m y^{-1}
M_T^*	annualised average of M_T	7 m y^{-1}
Q_E	evaporative heat flux	125 W m^{-2}
Q_i	net radiation	440 W m^{-2}
r_h	relative humidity	0.3
T_a	summer air temperature	283 K
T_M	melting temperature	273 K
T_∞	equilibrium temperature	297 K
κ_E	moisture diffusion coefficient	10^{-9} – $10^{-10} \text{ m}^2 \text{ s}^{-1}$
μ	defined in (7)	0.59
ρ_i	ice density	$0.9 \times 10^3 \text{ kg m}^{-3}$
ρ_w	water density	10^3 kg m^{-3}
σ	Stefan–Boltzmann constant	$5.67 \times 10^{-8} \text{ W m}^{-2} \text{ K}^{-4}$
ϕ	solid fraction	0.5
ΔT	defined in (11)	24.2 K

where s is the ice elevation surface, ρ_w is the water density, and η_w is the water viscosity. However, we do not pursue this topic here as such fluxes are small. From (1), we find

$$T = \frac{(kT_M + h_T h T_a) + h(Q_i - \sigma T^4)}{k + h_T h},$$

$$\rho_i L_m M = \frac{k(T - T_M)}{h} - \frac{\rho_w L_v \kappa_E (1 - r_h)}{h}; \quad (4)$$

the second of these is the latent heat generated at the ice surface.

We can estimate some of the terms using the values in table 1. First note that $\sigma T_M^4 \sim 315 \text{ W m}^{-2} \sim Q_i$. Debris temperatures can commonly reach 30 – $40^\circ\text{C} \sim 310 \text{ K}$, and this corresponds essentially to radiative equilibrium, $Q_i \approx \sigma T^4$; a value of $Q_i = 510 \text{ W m}^{-2}$ corresponds to a temperature of 35°C . We use this to define an equilibrium temperature

$$T_\infty = \left(\frac{Q_i}{\sigma} \right)^{1/4}. \quad (5)$$

Noting that $T_\infty - T_M \ll T_\infty$, (4)₁ can be written approximately¹ as

$$T \approx T_M + \frac{h[T_a - T_M + \mu(T_\infty - T_M)]}{h_a + (1 + \mu)h}, \quad (6)$$

¹Use (5) and the definition of μ in (7) to eliminate Q_i and σ in (1)₁, use the definition of h_a in (7) to eliminate k , expand $1 - (T/T_\infty)^4$ to first order in powers of $(T - T_\infty)/T_\infty$; simplifying the resultant expression for $T - T_M$ yields (6).

where

$$h_a = \frac{k}{h_T}, \quad \mu = \frac{4Q_i}{h_T T_\infty}. \quad (7)$$

Using (6) in (4), we have

$$\rho_i L_m M \approx \frac{k[T_a - T_M + \mu(T_\infty - T_M)]}{h_a + (1 + \mu)h} - \frac{\rho_w L_v \kappa_E (1 - r_h)}{h}; \quad (8)$$

the first term gives the predominant decaying trend of the Östrem curve, while the second gives the rising portion of the curve for small h .

Since air is an insulator, an appropriate choice of thermal conductivity would be $k = \phi k_s$, where k_s is the thermal conductivity of sediment, say $k_s = 2 \text{ W m}^{-1} \text{ K}^{-1}$, whence we would have $k = 1 \text{ W m}^{-1} \text{ K}^{-1}$ as in table 1, and consistent with measurements of [Juen et al. \(2013\)](#).

An issue concerns the limit of the evaporative heat flux as $h \rightarrow 0$. In this limit, the term κ_E/h in (8) should become κ_E/h_E when $h = 0$, where h_E is the effective thickness of a thin atmospheric boundary layer. We mimic this by replacing κ_E/h by $\kappa_E/(h + h_E)$, and we calibrate h_E by choosing

$$\frac{\rho_w L_v \kappa_E}{h_E} = Q_E, \quad (9)$$

whence (8) takes the final form

$$M = \frac{M_T h_a^*}{h + h_a^*} - \frac{(1 - r_h) M_E h_E}{h + h_E}, \quad (10)$$

where

$$\begin{aligned} h_a^* &= \frac{h_a}{1 + \mu}, & M_T &= \frac{h_T \Delta T}{\rho_i L_m}, \\ \Delta T &= T_a - T_M + \mu(T_\infty - T_M), & M_E &= \frac{Q_E}{\rho_i L_m}. \end{aligned} \quad (11)$$

Making the same modifications in the evaporation rate E , we can derive from (1) the expression

$$E = \frac{\delta(1 - r_h) M_E h_E}{h + h_E}, \quad (12)$$

where

$$\delta = \frac{\rho_i L_m}{\rho_w L_v} \sim 0.12, \quad (13)$$

which can be used in (2). M_T is a thermal melt rate scale, and M_E is an evaporative melt rate scale. Equally, h_T is a thermal conductive length scale, and h_E is an evaporative transport length scale. The equation (10) gives a very simple parametric description of the Östrem curve in terms of the climatically controlled parameters M_T , M_E , h_T and h_E , which we might relate to the surface roughness ([Cuffey and Paterson 2010](#), p. 155).

In order to roughly calibrate the values of these parameters, we follow the discussion of energy balance in [Cuffey and Paterson \(2010\)](#). The quantity Q_E is the evaporative heat flux for clean ice at zero relative humidity. On page 157 of their book, [Cuffey and Paterson \(2010\)](#) give a typical estimate for this of $Q_E(1 - r_h) = 25 \text{ W m}^{-2}$, when the

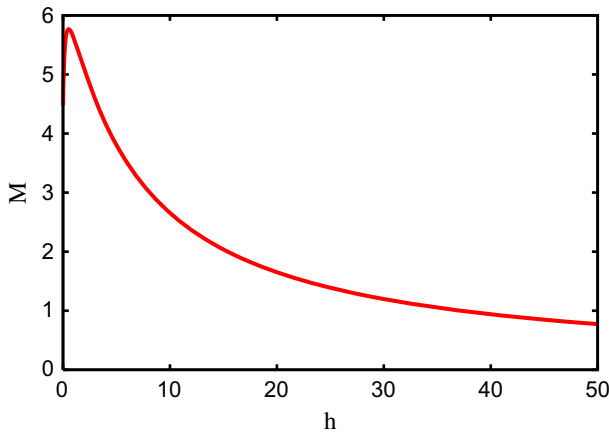


Figure 4. An Östrem curve for the melt rate M (m y^{-1}) as a function of debris depth h (cm). The function is that in (14), where the chosen parameter values are $M_T^* = 7 \text{ m y}^{-1}$, $M_E^* = 3.6 \text{ m y}^{-1}$, $h_a^* = 6.3 \text{ cm}$, $h_E = 0.2 \text{ cm}$, $r_h = 0.3$.

relative humidity is $r_h = 0.8$, and thus $Q_E = 125 \text{ W m}^{-2}$. It then follows that $M_E = 13.3 \text{ m y}^{-1}$.

At the same place, they suggest a sensible heat flux transfer coefficient of $h_T = 10 \text{ W m}^{-2} \text{ K}^{-1}$. A mean summer air temperature on Baltoro Glacier is 10°C , thus $T_a = 283 \text{ K}$, while if we select $Q_i = 440 \text{ W m}^{-2}$ following [Evatt et al. \(2015\)](#), then $T_\infty = 297 \text{ K}$, and thus $\Delta T = 24.2 \text{ K}$, using $\mu = 0.59$ computed from (7). Also from (7), $h_a = 0.1 \text{ m}$, and thus $h_a^* = 0.063 \text{ m}$, and from (11), $M_T = 25.7 \text{ m y}^{-1}$.

We now compare these (rough) estimates with actual data from Baltoro. The clean ice melt rate ranges between 4 and 7 cm d^{-1} , while the measured annual ablation is between 4 and 4.6 m y^{-1} . Further, the ablation season lasts 100 d, and this needs to be factored in. Relative humidity correlates inversely with temperature in the summer, and typical measured values of r_h are in the range 0.2–0.4 during warm days (when we suppose most melting occurs). If we take $r_h = 0.3$, then the clean ice melt rate from (10) is $M_T - 0.7M_E \approx 16.4 \text{ m y}^{-1}$, and dividing this by 365 yields an estimated clean ice melt rate of 4.5 cm d^{-1} . Astonishingly, this unforced estimate is entirely accurate.

In our modelling, we need to multiply the values of M_T and M_E by $100/365$, yielding (10) in the final form

$$M = \frac{M_T^* h_a^*}{h + h_a^*} - \frac{(1 - r_h) M_E^* h_E}{h + h_E}, \quad (14)$$

where $M_T^* \approx 7 \text{ m y}^{-1}$, $M_E^* \approx 3.6 \text{ m y}^{-1}$, and we use these values as a guide.

It remains to ascertain a suitable value for h_E . This can be obtained from (9), providing a suitable estimate for κ_E is given. Measurement of water vapour diffusivity in porous media is complicated by the soil suction associated with residual liquid saturation, and κ_E is much lower than the free air diffusivity. Measured values lie in the typical range 10^{-9} – $10^{-10} \text{ m}^2 \text{ s}^{-1}$ ([Rose 1963](#), figure 6), and lead to estimates of $h_E = 0.2$ – 2 cm .

As shown in figure 4, M initially increases with h (if h_E is low enough) before reaching a maximum and then decreasing towards zero as h increases. This figure is in fact remarkably similar to measured Östrem curves (see [Evatt et al. 2015](#), figure 2).

If we suppose that $h_E \ll h_a^*$, then M has a maximum at $h = h_M$, where

$$h_M = \frac{(\hat{h} - h_E)h_a^*}{h_a^* - \hat{h}}, \quad (15)$$

and

$$\hat{h} = \left[\frac{(1 - r_h)M_E^* h_E h_a^*}{M_T^*} \right]^{1/2} \quad (16)$$

(roughly the geometric mean of h_E and h_a^*); in particular if $h_E \ll h_a^*$, then $h_M \approx \hat{h}$.

Typical measured values of h_M are in the range 1–2 cm (Mattson *et al.* 1993, Kayastha *et al.* 2000), but it is noteworthy that in the experiments done to ascertain these and other Östrem figures (including Östrem's own), surfaces with prepared thicknesses of sands and gravels were used, for which we should expect the surface roughness to be small. Indeed, if $\hat{h} = 2$ cm, then $h_E \approx 2.5$ mm, consistent with the relatively smooth surfaces seen in, for example, figure 1 of Kayastha *et al.* (2000).

However, we think that on natural debris-covered surfaces, and particularly on Baltoro Glacier, where the debris cover is highly irregular and coarse-grained, the roughness length, and indeed other of the parameter choices, may be significantly different, so we allow some flexibility in our parameter choices below. In particular, increasing void space in the debris layer is liable to increase the vapour diffusivity somewhat towards its free air value, which is $2.6 \times 10^{-5} \text{ m}^2 \text{ s}^{-1}$ (Rose 1963), and the constraint in (9) would suggest a larger value of h_E also.

2.2. Mathematical model

Our task now lies in showing how the form of the Östrem curve will actually lead to the features which are seen. The basis of our model is that when the debris layer has a thickness which lies on the increasing portion of the Östrem curve, a uniform layer of debris cover promotes an instability, and the consequent evolution of the debris thickness can lead, in certain circumstances, to the formation of steep patches of clean ice, as the debris slides off. More specifically, we suppose that the thickness of the debris layer increases as the ice moves downstream. An initially thin debris cover will seed the initial growth of an ice sail, and its growth will not be limited until the debris cover becomes sufficiently thick that the melt rate of debris-covered ice becomes comparable to that of clean ice. For the melt rate portrayed in figure 4, where the clean ice melt rate is $\approx 4.5 \text{ m y}^{-1}$, this would be when $h \approx 3$ cm.

The geometry of the model is indicated in figure 5. We denote the elevation of the ice surface as s , and the thickness of the debris layer as h , and these are both functions of space \mathbf{x} and time t . The ice surface melts at a rate $M(h)$, which we take to depend on debris thickness but not on solar angle. In reality, north facing slopes will be subject to lower melting than south facing slopes, which in our simple two-dimensional theory would be accommodated by a dependence of M on ∇s . This effect is liable to be important in the formation of such asymmetric features as ice cliffs, but is ignored here as having secondary importance (it will affect the precise shape of ice sails, which is, however, not our principal concern. The ice surface also diffuses because a small amount of ice creep is driven by surface slopes, and this creep can be modelled by a diffusion term, with diffusion

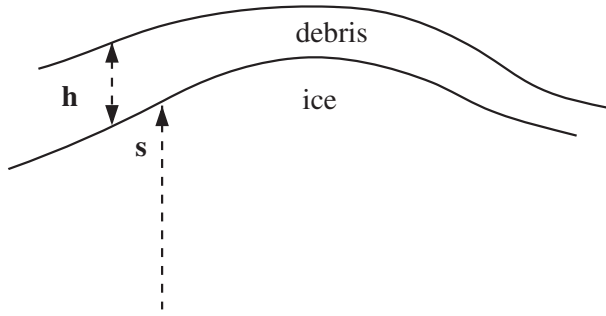


Figure 5. Geometry of the model.

coefficient D_i . We can estimate the value of D_i from a creep-derived estimate describing the viscous collapse of an ice dome; this gives

$$D_i \sim \frac{\rho_i g d^3}{3\eta_i}, \quad (17)$$

as follows from a straightforward application of lubrication theory (Acheson 1990, exercise 7.13), where ρ_i is ice density, g is the acceleration due to gravity, d is the depth of the ice dome, and η_i is ice viscosity. If we take values $\eta_i = 6 \text{ bar y} = 2 \times 10^{13} \text{ Pa s}$, $\rho_i = 0.9 \times 10^3 \text{ kg m}^{-3}$, $g = 10 \text{ m s}^{-2}$, $d = 10 \text{ m}$, this yields $D_i \sim 0.5 \text{ m}^2 \text{ y}^{-1} = 13.7 \text{ cm}^2 \text{ d}^{-1}$, but this is liable to be a severe overestimate, since the stress dependence of the viscosity will cause the viscosity to be significantly higher at the surface, where the shear stress vanishes. To accommodate this, we select a value of the viscosity 50 times lower, and then

$$D_i \sim 0.01 \text{ m}^2 \text{ y}^{-1} = 0.27 \text{ cm}^2 \text{ d}^{-1}, \quad (18)$$

and will be even lower for smaller ice domes. One commonly thinks of ice domes of this magnitude as stagnant; bear in mind that a one metre high ice pyramid would take significantly more than a century to flatten under this diffusion rate; so that in reality it would indeed be “stagnant ice”. Although, as it turns out, the ice creep term is relatively small, it is necessary to retain it in order to obtain a coherent asymptotic approximation.

We also assume that sediment cover creeps, and we also model this as a diffusive process, with diffusion coefficient D_s . This is a common assumption in geomorphology (McKean *et al.* 1993, Fernandes and Dieterich 1997). Most simply, it represents the inclination of unconsolidated sediment to roll down slopes. In the present case, the physical process has been described by Anderson (2000) in some detail. Diffusion occurs through the development and collapse of small scale ice tables under clasts. These form as the ice melts, since the covered ice is protected from melting. Eventually the clasts will topple, with a slight preference to roll downslope. Anderson also offers an estimate for the diffusivity, which in the present case we would interpret as

$$D_s \approx M_0 h, \quad (19)$$

where M_0 is the clean ice melting rate. Clearly the diffusive flux should go to zero as h goes to zero; also it should depend on surface slope, since the flux will become large on very steep slopes. However, for simplicity, we take $D_s \sim M_0 h_0$ to be constant, where h_0 is a typical value of the debris layer thickness. Taking values $M_0 \sim 5 \text{ m y}^{-1}$ and $h \sim 1\text{--}10 \text{ cm}$, this suggests

$$D_s \sim 0.05\text{--}0.5 \text{ m}^2 \text{ y}^{-1} = 1.4\text{--}13.7 \text{ cm}^2 \text{ d}^{-1}. \quad (20)$$

The model equations are thus taken to be

$$\begin{aligned} s_t &= -M(h) + D_i \nabla^2 s, \\ h_t &= D_s (\nabla^2 s + \nabla^2 h). \end{aligned} \quad (21)$$

Here the subscript t denotes a partial time derivative. These equations represent conservation of mass of ice and sediment, respectively: the ice flux is $-D_i \nabla s$, and the melt rate $M(h)$ represents loss of ice to meltwater (which is considered to be instantaneously removed from the system). The second equation is essentially an Exner equation, in which the flux of sediment is $-D_s \nabla (s + h)$, where the sediment is taken to creep down slopes of the till surface $z = s + h$.

3. Linear stability

We begin by non-dimensionalising the model. With h_0 being a representative debris thickness, we scale the variables as

$$s + M_c t \sim h_0, \quad h \sim h_0, \quad M = M_c + \Delta M m,$$

$$\mathbf{x} \sim l = \left(\frac{D_i h_0}{\Delta M} \right)^{1/2}, \quad t \sim t_0 = \frac{h_0}{\Delta M}, \quad (22)$$

where

$$\Delta M = M_c - M_0, \quad M_0 = M(0), \quad M_c = M(h_0), \quad (23)$$

and this leads to the dimensionless model²

$$\begin{aligned} s_t &= -m(h) + \nabla^2 s, \\ \varepsilon h_t &= \nabla^2 s + \nabla^2 h, \end{aligned} \quad (24)$$

where the dimensionless parameter is

$$\varepsilon = \frac{D_i}{D_s}. \quad (25)$$

For the choice of melt rate function given by (14), we have

$$m(h) = (h - 1) \left[\frac{1 + m^*}{1 + \Lambda h} - \frac{m^*}{1 + \lambda h} \right], \quad (26)$$

²More precisely, we write $s + M_c t = h_0 s^*$, $h = h_0 h^*$, etc., to obtain dimensionless equations for the starred variables. As is commonly done, we then immediately drop the asterisks as the discussion henceforth involves only the dimensionless variables.

where

$$\lambda = \frac{h_0}{h_a^*}, \quad \Lambda = \frac{h_0}{h_E}, \quad m^* = \frac{M_T^* h_0}{(h_0 + h_a^*) \Delta M},$$

$$\Delta M = \frac{(1 - r_h) M_E^* \Lambda}{1 + \Lambda} - \frac{M_T^* \lambda}{1 + \lambda} > 0. \quad (27)$$

For future reference, we note that $m(0) = -1$, $m(1) = 0$, and

$$m'(1) > 0 \quad \text{if} \quad m^* < \frac{1 + \lambda}{\Lambda - \lambda} \quad \text{or} \quad \lambda > \Lambda, \quad (28)$$

although we may discount the latter case since then $m(h)$ never decreases at large h .

If we take the values in (18) and (20), and also

$$h_0 = 1 \text{ cm}, \quad \Delta M = 1 \text{ m y}^{-1}, \quad (29)$$

then we have

$$l = 1 \text{ cm}, \quad t_0 = 0.01 \text{ y}. \quad (30)$$

The instability we seek will be on the scale of the debris layer thickness, and the time of formation of a bare ice patch may be over a melt season; this is what is observed, but nonlinear effects will be necessary to explain the enormous amplitudes of the sails, and their growth will take several melt seasons. The estimated value of ε is

$$\varepsilon \sim 0.02\text{--}0.2; \quad (31)$$

the precise value is very uncertain, but the only important fact in what we do is that we take ε to be small.

We solve (24) on a spatial domain S , and take the boundary conditions for (24) to be those of no flux at the boundary, thus

$$\mathbf{n} \cdot \nabla s = \mathbf{n} \cdot \nabla h = 0 \quad \text{on} \quad \partial S. \quad (32)$$

A consequence of this is that the total debris cover is conserved:

$$\frac{1}{S} \int_S h \, dS = \bar{h}, \quad (33)$$

which also follows from integration of (24)₂ over the domain S . The mean thickness \bar{h} can be taken to be one in our stability analysis, but we may allow it to vary later to describe the generally increasing thickness of sediment cover downstream (and thus, as time increases).

The dimensionless function $m(h)$ given by (26) is as portrayed in figure 6. Two requirements in our theory are $m'(1) > 0$ (so that the steady state is unstable) and $m(\infty) < -1$ (so that the sails eventually disappear), and these constraints are satisfied if

$$\frac{\lambda(1 + \Lambda)}{\Lambda - \lambda} < m^* < \frac{1 + \lambda}{\Lambda - \lambda}, \quad (34)$$

and our choice of coefficients in figure 6 is made to satisfy these constraints.

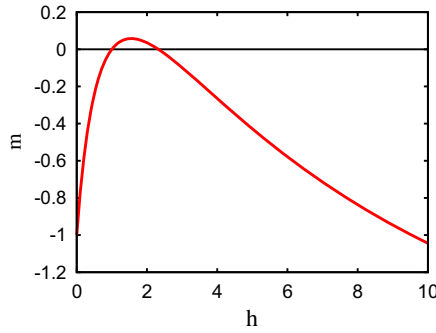


Figure 6. Typical assumed form of $m(h)$ given by (26). The parameters used are $h_0 = 1$ cm, $h_a^* = 6.3$ cm, $h_E = 1$ cm, whence $\Lambda = 1$, $\lambda = 0.16$, and also $m^* = 0.7$. With $M_T^* = 7$ m y^{-1} and $r_h = 0.3$, these choices correspond to $M_E^* = 3.26$ m y^{-1} , and also $\Delta M = 1.37$ m y^{-1} .

To assess the stability of a uniform state, we first note that (by choice of scales) a uniform solution of (24) is given by $h = 1, s = 0$, corresponding to a uniform debris thickness and a uniform melting rate of the ice surface. Note that there is another steady state with $h > 1$, but this is ruled out because the amount of debris is prescribed; we return to this in the following section.

Next we linearise the equations (24) about their uniform steady state solution and seek solutions $\propto \exp(\sigma t + i\mathbf{k}\cdot\mathbf{x})$, where \mathbf{k} is the wavenumber vector. The resulting equation for σ is the quadratic

$$\varepsilon\sigma^2 + k^2(1 + \varepsilon)\sigma - k^2[m'(1) - k^2] = 0, \tag{35}$$

whose solutions can be written in the approximate form (because $\varepsilon \ll 1$)

$$\begin{aligned} \sigma &= \sigma_+ \approx m'(1) - k^2, \\ \sigma &= \sigma_- \approx -\frac{k^2}{\varepsilon}. \end{aligned} \tag{36}$$

The second mode is stable, and represents the rapid relaxation of the debris surface due to sediment creep. However, if $m'(1) > 0$, the first mode is unstable to long wavelength perturbations, and we can expect undulations in debris thickness to grow on the time scale t_0 .

4. Finite amplitude sails

The form of the resulting patterns is relatively easily studied within the confines of this model, but there is an added subtlety. The sediment flux $-D_s \nabla(s + h)$ in (21) is clearly only non-zero if $h > 0$; if $h = 0$ the right hand side of (21)₂ should be taken to be zero. Most simply, this would be due to allowing D_s to depend on h , as suggested earlier. In our simpler version where D_s is taken as constant, we append the condition $h > 0$ to (21)₂, and thus also (24)₂.

Next, because $\varepsilon \ll 1$, (24)₂ rapidly relaxes to an equilibrium in which (because of the no flux boundary conditions)

$$s + h = Z(t) \quad \text{when} \quad h > 0, \quad (37)$$

where Z depends on time, and is the elevation of the debris surface (which is thus flat), and so h satisfies the non-linear Fisher-type equation (Fisher 1937), modulated by a debris conservation law:

$$\begin{aligned} h_t = m(h) + W + \nabla^2 h, & \quad \text{or} \quad h = 0 \quad \text{and} \quad s_t = 1 + \nabla^2 s, \\ \frac{1}{S} \int_S h \, dS = \bar{h}, & \quad W = \dot{Z}. \end{aligned} \quad (38)$$

Here \dot{Z} is the time derivative of $Z(t)$.

A major simplification of the problem results from noticing that if $h = 0$ (i.e. we are on a sail), then the height of the sail above the surrounding debris layer is

$$\tilde{h} = s - Z, \quad (39)$$

and thus satisfies

$$-\tilde{h}_t = -1 + W - \nabla^2 \tilde{h}, \quad (40)$$

and the condition of continuous ice flux ∇s at the sail boundary implies

$$\nabla \tilde{h} = -\nabla h \quad \text{when} \quad h = 0. \quad (41)$$

Now we notice a useful mathematical convenience: h is the dimensionless sediment thickness, and is thus non-negative. Equally \tilde{h} is the sail height, and only has meaning where there is no sediment. In our numerical solutions of the model, it is convenient to plot both functions on the same graph, with h directed downwards, as the resulting curve portrays the ice surface everywhere. Furthermore, we can see from (40) that $-\tilde{h}$ satisfies the *same* equation as h , providing we define $m(\tilde{h}) = -1$ for $\tilde{h} > 0$. Evidently we can thus extend the definition of h to $h < 0$ simply by defining

$$\tilde{h} = -h, \quad (42)$$

providing also we take $m(h) = -1$ for $h < 0$, and the integral constraint only integrates where $h > 0$:

$$h_t = m(h) + W + \nabla^2 h, \quad \frac{1}{S} \int_S \max(0, h) \, dS = \bar{h}. \quad (43)$$

In our figures below, we will plot $-h$ as thus defined, which delineates the ice surface everywhere.

Because the sails on Baltoro Glacier form a regular procession down the glacier, we will study the solutions of (43) in one spatial downstream dimension x . We suppose that there is a sail centred at $x = 0$, and $x = \pm L$ represents the mid-point before the next sail, centred

at $x = \pm 2L$. Thus we aim to solve

$$\begin{aligned} h_t &= m(h) + W + h_{xx}, \\ h_x &= 0 \quad \text{at} \quad x = 0, L, \quad \frac{1}{L} \int_0^L \max(0, h) \, dx = \bar{h}. \end{aligned} \tag{44}$$

The integral constraint represents the fact that the total debris volume is conserved. The subscript x denotes a partial derivative with respect to x (just as that for t does). The integral constraint makes this a non-standard problem whose form, however, has arisen in other contexts, where solutions have been obtained analytically and numerically (Budd *et al.* 1993, 1994, Fowler *et al.* 2007, Kyrke-Smith and Fowler 2014).

Let us suppose that $\bar{h} = 1$ (without any loss of generality). So long as $h > 0$ everywhere, we can integrate (44) from 0 to L , and using the boundary conditions, we then obtain (noting that the integral of h_t is zero)

$$0 = \int_0^L m(h) \, dx + WL. \tag{45}$$

If we take the specific case $m = -1 + h$, then $W = 0$ (as long as h remains positive). In a perturbation of the steady state $h = 1$ which conserves \bar{h} , the parts where $h > 1$ will increase, and the parts where $h < 1$ will decrease towards zero in finite time, thus forming the exposed sails. More generally, we will have $W \neq 0$, but the same conclusion holds: we expect sails to form as a consequence of the instability of the uniform state. In figure 7 we show the result of a numerical integration of the model (44), which bears out the description above. In interpreting this figure (which plots $-h$ vs. x in dimensional terms), recall that when $-h > 0$, $-h$ is the sail height above the sediment surface (from (39) and (42)), while when $-h < 0$ (or $h > 0$), h is the sediment depth. Thus the plot in figure 7 shows the ice sail ($-h > 0$) growing above its surrounding sediment cover ($-h < 0$) just as in nature.

For the case of a single sail in $-L_S < x < L_S$ (i.e. $x = \pm L_S$ are the edges of the sail where the debris layer begins), integration of (44)₁ leads to the definition of W as

$$W = A + \frac{1}{L} \left[\frac{d}{dt} \int_0^{L_S} h \, dx - \int_0^L m(h) \, dx \right], \tag{46}$$

where we include an *accretion rate* term $A = \dot{\bar{h}}$ to accommodate an increasing thickness of debris as the sails move downglacier, either through surface accumulation via rockfalls, or due to debris melt out from the ice; it follows that the system (44) is equivalent to

$$\begin{aligned} v_t &= A + m(h) - \frac{1}{L} \int_0^L m(h) \, dx + v_{xx}, \\ v_x &= 0 \quad \text{at} \quad x = 0, L, \end{aligned} \tag{47}$$

where

$$v = h - \frac{1}{L} \int_0^{L_S} h \, dx, \tag{48}$$

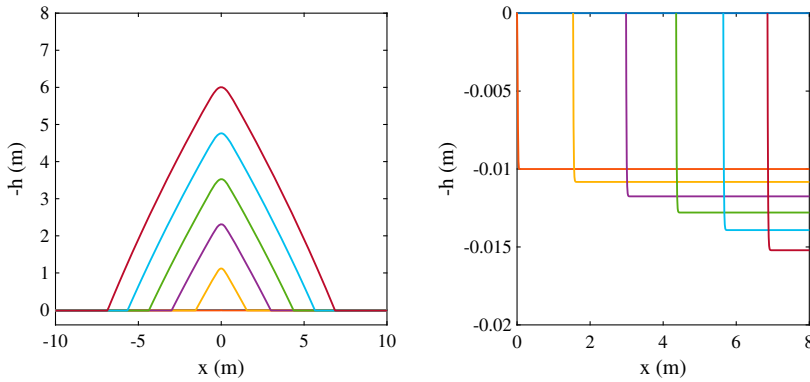


Figure 7. A sequence of plots of the evolving sails, obtained by solving (47) with (49) using $m(h)$ given by (26) (and $m = -1$ for $h < 0$), at times $t = 0, 0.4, 0.8, 1.2, 1.6, 2$ y. Where $-h > 0$, its value represents the height of the sail above the sediment surface ($-h = 0$), and where $-h < 0$, its value gives the elevation of the ice surface relative to the sediment surface. Both length and height are in metres. Parameter values used are $\lambda = 0.16$, $\Lambda = 1$, $m^* = 0.7$, as in figure 6, the accretion rate is $A = 0$, and the dimensional value of the half-spacing between sails is $L_d = 20$ m. The length and time scales are as in (30), i.e. $l = 1$ cm, $t_0 = 0.01$ y; thus $L = 2,000$. The dimensionless time and space steps were both 0.1, and the initial condition for till thickness was (in dimensionless terms) $h = 1 - \exp(-0.2x^2)$, thus a layer of thickness 1 cm with a small thinner patch around 7 cm wide. The left hand plot shows the growing ice sail, whose height is given by $-h$. Where $h > 0$ (right hand plot), this gives the debris thickness. The axis $-h = 0$ is the surface of the debris layer. The close up on the right shows that away from the sail, the debris layer is of uniform thickness, and slowly deepens with time.

and thus

$$h = v + \frac{1}{(L - L_S)} \int_0^{L_S} v \, dx. \quad (49)$$

This is straightforward to solve numerically; v is stepped forward from (47) with an implicit finite difference approximation, and then h updated from (49), with L_S being given by linear interpolation between the grid points where h passes through zero; the integrals are computed using the trapezium rule. The time step is iterated to determine the updated value of L_S where $h = 0$. In computing the figure shown, three iterations of the time step were used, and the time and space steps were $\Delta t = 0.1$ and $\Delta x = 0.1$. Finer choices of the mesh made little difference to the results. Our choice of the boundary values of v was chosen to conserve debris mass rather than zero flux (though they are theoretically equivalent).

5. Discussion

The numerical solution shown in figure 7 shows that sails of the observed size will grow in a few years. Despite the simplicity of the model, they even have the right shape. If the computation in figure 7 is carried on further, the sails eventually reach an equilibrium. The cause of this is that the residual debris thickness increases as it is squeezed into a smaller length ($L - L_S$), so that eventually (see figure 6) $m = -1$ for $h \approx 10$ cm, and the sails melt as rapidly as the debris-covered ice. For a larger spacing, the size of the sails is correspondingly larger.

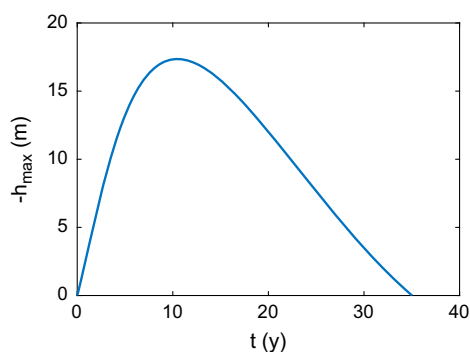


Figure 8. Evolution of maximum sail height (m) as a function of time (y). Parameters as for figure 7 but with a dimensionless accretion rate of $A = 0.001$, corresponding to 0.1 cm y^{-1} .

In reality, debris accretes as the sails progress downstream, and if we suppose a mean thickness of 10 cm accretes over a sail lifetime of $\sim 100 \text{ y}$ (Evatt *et al.* 2017), this represents an annual accretion rate of 0.1 cm y^{-1} , and dimensionlessly $A = 0.001$. Figure 8 shows the evolution of the maximum sail height with time for a value of $A = 0.001$, when the sail lifetime is actually about 35 years.

It is evident from the theory and the computations that if the melt or wastage rate of ice $M(h)$ in figure 4 as a function of debris cover thickness h exhibits the Östrem property, that is, M first increases before decreasing, as in figure 4, then bare ice patches will grow relative to thinly covered ice. Whether sails then grow to amplitudes of metres then depends largely on how much lower the bare ice melting rate is. If it is significantly less than the peak melting rate, then sails will continue to grow until the debris increases sufficiently to catch up. Thus the issue is not the range of debris thickness where the melt rate is increasing, but the lowering of the bare ice melting rate.

Adopting (14) as our Östrem melt rate, we see that this lowering is essentially given by $(1 - r_h)M_E^*$, and this quantity is distinguished on Baltoro Glacier by the generally low value of the relative humidity $r_h \approx 0.3$, which has the required effect. Since direct observation tells us that the bare ice melt rate is a metre a year less than that of ice covered with debris to a typical depth of 10 cm, it seems the Östrem curve on Baltoro does have this property.

It is also evident from the model that an even simpler model could have been used, since in practice the diffusive term in the computations is largely irrelevant (except at the sail edge), and the only issue is the difference in melt rate of the sail and of the debris-covered ice.

6. Conclusions

We have shown that a very simple model of differential ablation based on the thickness of supraglacial debris can lead to an instability, if the debris thickness is sufficiently thin that it lies on the increasing portion of the presumed Östrem ablation curve, and that the result of this instability can be the ice sails which have been observed on glaciers in the Karakoram. In passing, we have provided a simple formulation of the Östrem curve, which appears consistent with measured values.

Theoreticians have conventionally viewed the ice upper surface as an essentially flat (and clean) interface, just as in times past they viewed the glacier bed in the same way. And just as theoreticians now deal routinely with the glacier bed as a corrugated interface between ice, water and till, in the future they will need to consider the glacier surface in the same way. In particular, debris-covered glaciers are not flat, and the variety of surface forms which are observed poses significant theoretical challenges. The formation of ice sails is just one of many such challenges in the study of supraglacial geomorphology.

Acknowledgements

This paper is the result of a workshop held in Grasmere, Lake District, England, 30 September–4 October 2013. Funding for the workshop was provided by the Engineering and Physical Sciences Research Council, UK, via the MAPLE Platform Grant EP/I01912X/1. A. C. F. acknowledges the support of the Mathematics Applications Consortium for Science and Industry (www.macsi.ul.ie) funded by the Science Foundation Ireland mathematics grant 12/1A/1683. Special thanks to Geoff Evatt for organising the event, and to the other members of the workshop for their contributions: Dave Abrahams, Matthias Heil, Jonny Kingslake, Lindsey Nicholson, Jack Holt and Katie Joy. A special mention also for Astrid Pacini, who worked tenaciously on this problem as a visiting undergraduate student from Yale to Oxford during the summer of 2014.

Disclosure statement

No potential conflict of interest was reported by the authors.

Funding

This work was supported by the Engineering and Physical Sciences Research Council, UK, via the MAPLE Platform [grant number EP/I01912X/1]; Science Foundation Ireland mathematics [grant number 12/1A/1683].

References

- Acheson, D.J., *Elementary Fluid Dynamics*, 1990 (O. U. P.: Oxford).
- Anderson, R.S., A model of ablation-dominated medial moraines and the generation of debris-mantled glacier snouts. *J. Glaciol.* **2000**, **46**, 459–469.
- Benn, D.I., Bolch, T., Hands, K., Gulley, J., Luckman, A., Nicholson, L.I., Quincey, D., Thompson, S., Toumi, R. and Wiseman, S., Response of debris-covered glaciers in the Mount Everest region to recent warming, and implications for outburst flood hazards. *Earth Sci. Revs.* **2012**, **114**, 156–174.
- Bolch, T., Kulkarni, A., Kääb, A., Huggel, C., Paul, F., Cogley, J.G., Frey, H., Kargel, J.S., Fujita, K., Scheel, M., Bajracharya, S. and Stoffel, M., The state and fate of Himalayan glaciers. *Science* **2012**, **336**, 310–314.
- Brun, F., Buri, P., Miles, E.S., Wagnon, P., Steiner, J., Berthier, E. and Pellicciotti, F., Quantifying volume loss from ice cliffs on debris-covered glaciers using high-resolution terrestrial and aerial photogrammetry. *J. Glaciol.* **2016**, **62**, 684–695.
- Budd, C., Dold, B. and Stuart, A., Blowup in a partial differential equation with conserved first integral. *SIAM J. Appl. Math.* **1993**, **53**, 718–742.
- Budd, C.J., Dold, J.W. and Stuart, A.M., Blow-up in a system of partial differential equations with conserved first integral. Part II: problems with convection. *SIAM J. Appl. Math.* **1994**, **54**, 610–640.
- Cuffey, K.M. and Paterson, W.S.B., *The Physics of Glaciers*, 4th ed., 2010 (Elsevier: Amsterdam).
- Evatt, G.W., Abrahams, I.D., Heil, M., Mayer, C., Kingslake, J., Mitchell, S.L., Fowler, A.C. and Clark, C.D., Glacial melt under a porous debris layer. *J. Glaciol.* **2015**, **61**, 825–836.

- Evatt, G.W., Mayer, C., Mallinson, A., Abrahams, I.D., Heil, M. and Nicholson, L., The secret life of Ice Sails. *J. Glaciol.* **2017**, submitted.
- Fernandes, N.F. and Dieterich, W.E., Hillslope evolution by diffusive processes: the timescale for equilibrium adjustments. *Water Resour. Res.* **1997**, **33**, 1307–1318.
- Fisher, J.E., Ice pyramids on glaciers. *J. Glaciol.* **1950**, **1**, 373–377.
- Fisher, R.A., The wave of advance of advantageous genes. *Ann. Eugenics* **1937**, **7**, 353–369.
- Fowler, A.C., Kopteva, N. and Oakley, C., The formation of river channels. *SIAM J. Appl. Math.* **2007**, **67**, 1016–1040.
- Juen, M., Mayer, C., Lambrecht, A., Wirbel, A. and Kueppers, U., Thermal properties of a supraglacial debris layer with respect to lithology and grain size. *Geogr. Ann. A* **2013**, **95**, 197–209.
- Juen, M., Mayer, C., Lambrecht, A., Han, H. and Liu, S., Impact of varying debris cover thickness on ablation: a case study for Koxkar Glacier in the Tien Shan. *The Cryosphere* **2014**, **8**, 377–386.
- Kayastha, R.B., Takeuchi, Y., Nakano, M. and Ageta, Y., Practical prediction of ice melting beneath various thickness of debris cover on Khumbu Glacier, Nepal, using a positive degree-day factor. *IASH Publ.* **2000**, **264**, 71–81.
- Kotlyakov, V.M. and Lebedeva, I.M., Nieve and ice penitentes, their way of formation and indicative significance. *Z. Gletsch.kd. Glazialgeol.* **1974**, **10**, 111–127.
- Kyrke-Smith, T.M. and Fowler, A.C., Subglacial swamps. *Proc. R. Soc. Lond. A* **2014**, **470**, 20140340.
- Lliboutry, L., The origin of penitents. *J. Glaciol.* **1954**, **2**, 331–338.
- Mattson, L.E., Gardner, J.S. and Young, G.J., Ablation on debris covered glaciers: an example from the Rakhiot Glacier, Punjab. Himalaya. *IAHS Publ.* **1993**, **218**, 289–296.
- Mayer, C., Lambrecht, A., Belo, M., Smiraglia, C. and Diolaiuti, G., Glaciological characteristics of the ablation zone of Baltoro glacier, Karakoram. Pakistan. *Ann. Glaciol.* **2006**, **43**, 123–131.
- McKean, J.A., Dietrich, W.E., Finkel, R.C., Southron, J.R. and Caffee, M.W., Quantification of soil production and downslope creep rates from cosmogenic ¹⁰Be accumulations on a hillslope profile. *Geology* **1993**, **21**, 343–346.
- Nakawo, M., Iwata, S., Watanabe, O. and Yoshida, M., Processes which distribute supraglacial debris on the Khumbu Glacier, Nepal Himalaya. *Ann. Glaciol.* **1986**, **8**, 129–131.
- Nicholson, L. and Benn, D.I., Properties of natural supraglacial debris in relation to modelling sub-debris ice ablation. *Earth Surf. Proc. Landf.* **2013**, **38**, 490–501.
- Östrem, G., Ice melting under a thin layer of moraine, and the existence of ice cores in moraine ridges. *Geogr. Ann.* **1959**, **41**, 228–230.
- Reid, T.D. and Brock, B.W., Assessing ice-cliff backwasting and its contribution to total ablation of debris-covered Miage glacier, Mont Blanc massif, Italy. *J. Glaciol.* **2014**, **60**, 3–13.
- Rose, D.A., Water movement in porous materials: Part 1 – Isothermal vapour transfer. *Brit. J. Appl. Phys.* **1963**, **14**, 256–262.
- Rowan, A.V., Egholm, D.L., Quincey, D.J. and Glasser, N.F., Modelling the feedbacks between mass balance, ice flow and debris transport to predict the response to climate change of debris-covered glaciers in the Himalaya. *Earth Planet. Sci. Letts.* **2015**, **430**, 427–438.
- Sakai, A., Nakawo, M. and Fujita, K., Distribution characteristics and energy balance of ice cliffs on debris-covered glaciers, Nepal Himalaya. *Arct. Antarct. Alpine Res.* **2002**, **34**, 12–19.
- Steiner, J.F., Pellicciotti, F., Buri, P., Miles, E.S., Immerzeel, W.W. and Reid, T.D., Modelling ice-cliff backwasting on a debris-covered glacier in the Nepalese Himalaya. *J. Glaciol.* **2015**, **61**, 889–907.
- Swithinbank, C., The origin of dirt cones on glaciers. *J. Glaciol.* **1950**, **1**, 461–465, 439.
- Visser, Ph.C., Gletscherüberschiebungen im Nubra- und Shyok-Gebiet des Karakorum. *Z. Gletsch.* **1932**, **20**, 29–44.